Structure and Dynamics of the Aniline−Argon Complex as Derived from its Potential Energy Surface

Jan Makarewicz[†]

Faculty of Chemistry, A. Mickiewicz University, Grunwaldzka 6, PL 60-780 Poznań, Poland

Received: August 24, 2006; In Final Form: December 11, 2006

The structure and dynamics of the van der Waals (vdW) complex of aniline (An) with argon (Ar) are studied using ab initio methods. The inversion potential of the aniline−argon (AnAr) complex perturbed by the weak vdW interaction is calculated taking into account subtle corrections from the zero-point energy of the vdW modes and from the frequency shifts of the An normal modes modified by the complexation. The intermolecular potential energy surface (PES) of the AnAr complex is determined by performing a large-scale computation of the interaction energy and the fitting of the analytical many-body expansion to the set of single-point interaction energies. The PES determined shows two deep local minima corresponding to the *anti* and *syn* AnAr conformers. The difference in the energies of these two minima is only 15 cm^{-1}, but it is sufficient to localize the inversion wave functions and to form the two conformers. In the conformer *anti* (*syn*) of lower (higher) energy, Ar is bound to the An ring opposite (adjacent) the amino-hydrogens. In the additional local minima higher in energy, Ar approaches the aniline ring between the C−H bonds near its plane. An additional local minimum is located opposite of nitrogen between the two N−H bonds. The high-energy minima are, however, too flat to form stable conformers. The perturbation of the interaction of Ar with the phenyl ring by the NH_2 group is described by the vdW hole, which is responsible for unusually strong intermode mixing in the excited intermolecular vibrational states. The analysis of these states calculated for the ground (S_0) as well as the first excited electronic state (S_1) resolves difficulties faced earlier with the assignment of the observed vibronic bands of AnAr.

I. Introduction

The complexes of aromatic molecules with rare gas atoms are bound by weak van der Waals (vdW) interactions, which determine many fundamental chemical and physical phenomena such as conformations of biomolecules, the structures of molecular crystals, solvation and adsorption of molecules, and so forth. The aniline−argon (AnAr) complex is of particular interest because its conformers can be created by the weak intermolecular interaction that perturbs the large-amplitude inversion motion of the amino (NH_2) group in the aniline (An) monomer. This complex is an important model system investigated intensively from both experimental and theoretical point of views. The experimental data on the structure,[1−5] frequencies of the intermolecular vdW vibrational modes,[6−10] binding energy and its change under electronic excitation[6,8,11−14] ionization potentials,[8,10,15] intramolecular vibrational energy redistribution, and vibrational predissociation[3,12,15,16] have been provided by the studies of the ground (S_0) and the first excited (S_1) electronic states of the AnAr complex in the neutral and cationic forms. Larger $AnAr_n$ clusters involving several Ar atoms have also been intensively investigated experimentally[7,13,17−19] and theoretically.[20−22]

The information on the AnAr cluster was difficult to interpret because of complexity of the AnAr dynamics caused by the inversion motion of the An amino group and three vdW intermolecular motions involving Ar. The spectra of the bare An molecule revealed that the inversion of the amino group is driven by the symmetric double well potential.[23−27] In the presence of Ar, this symmetric potential converts into an asymmetric double well potential, which can localize the amino hydrogens above or below the An ring plane. As a result, two conformers of AnAr can appear. The Ar atom can be attached to the ring either on the same side (*syn* conformer) or on the opposite side (*anti* conformer) with respect to the out-of-plane hydrogens of the NH_2 group. Becucci et al.[2] extracted the structural parameters from the rotationally resolved S_1-S_0 fluorescence excitation spectra of AnAr and assumed the theoretical model of this complex with the *syn* conformer as the most stable. Alternatively, Sinclair and Pratt[3] independently observed the S_1-S_0 spectra of AnAr and concluded from their experiment that the *anti* conformer is the most stable. These two pictures have been supported or criticized by other authors.[4,5,21,28,29]

The relative stability of AnAr conformers cannot be precisely determined without solving the problem of the dynamics of the complex governed by its global potential energy surface (PES) describing the vdW motions of Ar and their interaction with the vibrational modes of the An monomer. Such a solution is necessary to estimate the vibrational zero-point energy (ZPE) of the vdW and intramolecular monomer modes for the *anti* and *syn* minima in the PES. The ZPE of the vdW modes could be derived from the band frequencies observed in the vibronic spectra. The frequencies corresponding to such modes have been measured for ground (S_0) and the excited electronic state (S_1). However, there is still controversy about the assignment of the spectra observed because three mutually exclusive assignments of the vibronic spectra have been reported.[6,7,9,30]

The goal of this paper is to resolve controversies about the structure and dynamics of the AnAr complex whose features

[†] Fax: (4861) 865-80-08; phone: (4861) 829 1392; e-mail: jasiu@rovib.amu.edu.pl.

10.1021/jp0654866 CCC: $37.00
Published on Web 02/06/2007

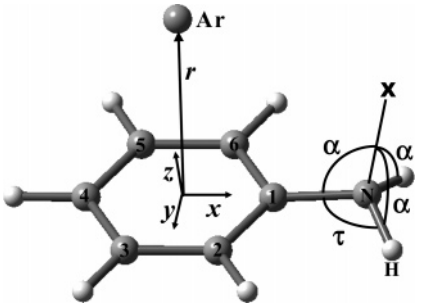

Figure 1. Molecular system of axes *x*, *y*, and *z* used to define the Ar position vector **r**, and the angular coordinates α and τ of the NH_2 group.

depend on the localization of its inversion wave functions. For this reason, we first investigate a simpler problem of the inversion motion in the unperturbed An monomer. In Section II, a flexible model is defined for an adequate description of this motion. The inversion dynamics is determined by two crucial factors; the inversion barrier height and the equilibrium structure of two symmetrically equivalent potential minima. This structure is calculated using ab initio methods for An in the ground (S_0) and excited (S_1) electronic states. In Section III, the An inversion barrier is estimated accurately using high-level ab initio methods. The inversion potential function perturbed by the vdW interaction in the AnAr complex is studied in Section IV.

The assignment problem of the vdW vibrational modes can be resolved knowing a highly accurate intermolecular PES. Thus, in Section V we perform ab initio calculations of the An−Ar interaction energy to construct the analytical PES. In Section VI, the dynamical problem of the vdW intermolecular motions of the complex is solved numerically for the ground (S_0) and the first excited (S_1) electronic states. A comparison of the calculated vdW vibrational frequencies with the experimental ones allows us to establish a proper assignment of the observed bands. Section VII presents a concluding summary.

II. Aniline Equilibrium Structure and the Flexible Model of the Inversion Motion

The AnAr complex exhibits the small-amplitude vibrations (SAVs) of the An monomer, the large-amplitude inversion motion of the amino group, and three intermolecular vdW vibrations. The inversion motion interacts with SAVs and vdW vibrations. A complete rigorous dynamical treatment of all vibrational modes is unfeasible. Thus, approximate models appeared to be unavoidable. The first proposed dynamical model of the An monomer included the inversion mode as a dynamical variable, whereas all SAVs were frozen out.[23−27] Such a rigid model has been extended by including the NH_2 inversion and torsion motions.[31] However, the features of the inversion motion interacting with the remaining modes can be better described using the flexible model in which the SAV coordinates are considered as geometry parameters dependent adiabatically on the inversion coordinate. A simplified model of this kind has been applied to the An monomer by Bludsky et al.[32]

In our problem, a full relaxation of the AnAr geometry along the minimum energy path of the inversion mode has to be considered because it may affect a small difference in the energies of the two AnAr conformers. To describe all possible deformations of the An ring and of the amino group during the inversion motion, we introduce the umbrella-like coordinates[33,34] that define uniquely an instantaneous configuration of a set of four arbitrary nuclei. They are illustrated in Figure 1 for the NH_2 group connected to the carbon C_1 of the An ring. The inversion coordinate is the angle α defined in conjunction with the local axis system based on the four nuclei C_1NHH', with the origin at the central nucleus N. The N−X axis of this system makes the same angle α with the three bonds: NC_1, NH, and NH′, cf. Figure 1. Thus, the N−X axis is a trisector of the pyramid formed by the four chosen nuclei. For the planar C_1NHH' configuration, $\alpha = \pi/2$, so we can introduce a more convenient angle $\rho = \pi/2 - \alpha$ which is zero for the planar configuration, $\rho > 0$ ($\rho < 0$) for the hydrogens H and H′ located above (below) the An ring. Additionally, the two twisting angles τ and τ' are necessary to specify the orientations of the two NH bonds. The angle τ (τ') is defined as the dihedral angle between the plane HNX (H′NX) and NXC_1. Analogous inversion angles ρ_1 and ρ_2 based on the central C_1 and C_4 atoms, respectively, are defined to specify the ring nonplanarity.

In the earlier An models, the inversion angle has been defined as the angle β' between the ring and NH_2 planes. However, our calculations show that the ring is slightly nonplanar, so the angle β between the C_1N direction and the NH_2 bisector would be more convenient. This angle is related to α by $\beta = \pi - a\tan(\tan\alpha\cos\tau)$.

The position of the Ar atom in the complex is specified by the Cartesian (*x*,*y*,*z*) or the corresponding spherical (r,θ,ϕ) coordinates measured with respect to the axis system with the origin at the An ring center (RC), which is the middle point between C_1 and C_4. The *x* axis connects C_4 and C_1 and is directed toward the C_1 atom. The *y* axis is perpendicular to the *x* axis and parallel to C_6-C_2. The *z* axis is perpendicular to the *x* and *y* axes.

To describe the inversion motion in the AnAr complex adequately, we investigate first a simpler problem of the inversion in the An monomer with the aim of determining the accurate equilibrium inversion angle β_e and the inversion barrier V_b. The experimental values of these important parameters are charged with large errors depending on the experimental data and models used to extract β_e and V_b. The angle β_e has been determined as $37.3 \pm 2°$ from the microwave data on the assumption that C_1N bond lies in the An ring plane,[35] whereas the far-infrared data yielded a β_e of $42 \pm 1°$.[26]

Ab initio calculations of the equilibrium geometry of aromatic molecules in their ground electronic states provide satisfactory results already at the level of second-order Møller−Plesset perturbation (MP2) theory. To optimize the An geometry, we use here the standard cc-pVTZ basis set.[36] All of the calculations are carried out using the GAUSSIAN 03 program.[37] The An equilibrium geometry in the S_0 electronic state calculated at the MP2/cc-pVTZ level compares well to the corresponding experimental r_s structure,[35] and the geometry parameters of the NH_2 group are expected to be more accurate than the experimental ones. The calculated equilibrium inversion angle $\rho_e = 16.5°$ corresponds to $\beta_e = 45.5°$ and to $\beta'_e = \beta_e - \gamma_e = 42.6°$.

The interpretation of the vibronic spectra of An and AnAr requires the knowledge of the equilibrium geometry of An in its first excited electronic state (S_1). Holas et al.[38] deduced from the inversion frequencies observed in the S_1-S_0 vibronic bands that An becomes nearly planar in the S_1 state. Very few ab initio studies have been carried out to describe the properties of this state. Recently, a series of An singlet excited states has been studied theoretically; however, the An structure has been assumed to be the same in all electronic states.[39]

In this paper, we use the complete active space self-consistent field (CASSCF) method[40−42] to optimize the An geometry in the S_1 state. A good description of this state requires the selection

of a proper active space. Initial calculations on the CIS level have revealed that the electronic configurations contributing to the S_1 state involve π orbitals of a_2 and b_1 symmetry species for a planar An molecule with C_{2v} point group symmetry. Thus, the three highest occupied orbitals (b_1,a_2,b_1) and two virtual orbitals (a_2,b_1) were included into the active space to perform the calculations CASSCF(6,5) on the S_1 state of B_2 symmetry type. The same active space was also used for nonplanar structures with lower symmetry.

The An structure in the S_1 state optimized at the CASSCF-(6,5)/cc-pVTZ level appears to be planar with the C−N bond significantly shortened and the extended ring. The excitation also changes the electric properties of the An molecule. Our calculations predict an increase in the dipole moment from 1.46 D in the S_0 state to 2.76 D in the S_1 state. These values agree well with the experimental counterparts of 1.52 and 2.80 D,[43] correspondingly.

III. Inversion Motion of Aniline

Experimental estimates of the An inversion barrier V_b range from about 450 to 560 cm^{-1}. For this reason, several ab initio studies of An have been undertaken to determine the V_b value more accurately. The sensitivity of the geometry and of V_b to the basis-set size and the correlation level of theory has been studied extensively by Bludsky et al.[32] Recently, a series of correlation-consistent basis sets cc-pV*X*Z, augmented by diffuse functions (aug-cc-pV*X*Z) and supplemented by tight functions adapted to core−core correlation[44] (cc-pCV*X*Z) up to $X = 4$ has been used to study the amino group nonplanarity in nucleic bases by Wang and Schaefer.[45] Their results demonstrated that the quadruple-ζ ($X = 4$) quality basis set was necessary to calculate reliable V_b values.

To compare the theoretical inversion barrier with the experimental one, the effect of the SAVs should also be investigated because the effective inversion potential energy function $V_{inv}(\rho)$ includes the contribution from SAV frequencies $\nu_k(\rho)$ dependent on the inversion coordinate[46]

$$V_{inv}(\rho) = V^0(\rho) + h\sum_k \nu_k(\rho)(n_k + 1/2) \qquad (1)$$

where $V^0(\rho)$ is the usual Born−Oppenheimer potential energy calculated along ρ, and n_k are SAV quantum numbers. Until now, the SAV contribution to the An inversion barrier V_b has not been considered. Here, this contribution is determined by calculating the SAV frequencies for the minimum [$\nu_k(\rho = \rho_e)$] and for the transition state TS [$\nu_k(\rho = 0)$] corresponding to the planar An molecule.

The frequencies of the SAV normal modes can be calculated accurately at a low computation cost by employing the density functional theory. Recently, a wide variety of basis sets and exchange-correlation functionals have been tested in calculations of the fundamental frequencies.[47−49] Triple-ζ basis sets with polarization functions already provided accurate results, and the B97−1 functional[50] was recommended for the calculations of the vibrational frequencies of aromatic molecules. The An vibrational frequencies calculated at the B97-1/cc-pVTZ level for the minimum and the transition state are scaled by the factors recommended in refs 51−53 agree well with the experimental data.[14,54−56]

According to eq 1, the SAV correction to V_b is the difference between the ZPE of the transition state and of the minimum

$$\Delta V_b(\mathrm{SAV}) = h\sum_k [\nu_k(0) - \nu_k(\rho_e)]/2 \qquad (2)$$

TABLE 1: Aniline Inversion Barrier V_b^0 (cm^{-1}) Calculated at the MP2/cc-pVTZ Optimized Geometries of the Minimum and Transition State Using Various Correlation Consistent Basis Sets

bazis set	HF	MP2
cc-pVDZ	641.5	820.7
cc-pVTZ	455.0	584.8
cc-pVQZ	410.5	496.0
aug-cc-pVDZ	471.6	501.8
aug-cc-pVTZ	377.1	456.0
aug-cc-pVQZ	363.0	406.9
basis set limit	363.0	381.9
ΔV_b^0(MP2)[b]		18.9
	HF	MP2(full)[a]
cc-pCVDZ	643.9	814.9
cc-pCVTZ	458.7	553.5
cc-pCVQZ	410.5	453.6
aug-cc-pCVDZ	465.4	493.3
aug-cc-pCVTZ	379.8	432.5
aug-cc-pCVQZ	363.5	368.6
basis set limit	363.5	333.8
ΔV_b^0(MP2)[b]		−29.7
ΔV_b^0[CCSD(T)][c]		94.7
ΔV_b^0(SAV)		64.0
total V_b^0		492.5

[a] Core orbitals are included in the correlation calculation of V_b^0. [b] MP2 correlation correction to V_b^0. [c] CCSD(T) correlation correction to V_b^0.

This correction of 64 cm^{-1} as determined from the calculated frequencies appears to be an essential contribution to V_b.

The values of the electronic contribution $V_b^0 = V^0(0) - V^0(\rho_e)$ to the inversion barrier calculated at the MP2 level using a series of the cc-pV*X*Z and aug-cc-V*X*Z basis sets for the cardinal number $X = 2$, 3 and 4, that is, D, T, and Q, are presented in Table 1. The results obtained with frozen core orbitals show the same trends as those observed in the case of nucleic bases with the amino group.[45] The barrier height V_b^0 systematically diminishes with the extension of the basis-set size. The augmentation of the cc-pV*X*Z basis sets by diffuse functions essentially improves the results. The aug-cc-pVDZ basis already yields a V_b^0 value very close to that obtained using large cc-pVQZ basis. Moreover, the augmented series provides less variation in the inversion barrier in comparison to the cc-pV*X*Z series, so the MP2 basis-set limit for V_b^0 can be estimated accurately using the results obtained already for $X = 3$ and 4. A simple and reliable method proposed by Helgaker et al.[57] for the estimation of the correlation energy at the basis-set limit needs only two correlation energy values ΔE_{corr}^X and ΔE_{corr}^Y calculated for the cardinal numbers X and Y of the basis sets. Using the MP2 and HF results for the aug-cc-pVTZ ($X = 3$) and aug-cc-pVQZ ($X = 4$) bases, we obtain, according to the recipe of ref 57, the correlation correction ΔV_b^0 of 18.9 cm^{-1}. The HF limit of V_b^0 is close to its HF/aug-cc-pVQZ value of 363 cm^{-1}, cf. Table 1; thus, the MP2 limit of V_b^0 is 382 cm^{-1}.

However, in the above evaluation the effect of the core correlation is neglected. To include the contribution to the inversion barrier created by this effect, the aug-cc-pCV*X*Z basis sets with tight basis functions designed for core−core and core−valence correlations are applied. The MP2(full) limit of ΔV_b^0 is determined from the extrapolation using the results obtained with the aug-cc-pCV*X*Z basis sets for $X = 3$ and 4. The total correlation correction ΔV_b^0 approaches the limit of −29.7 cm^{-1}. It is interesting to note that the core correlation contribution dominates and it lowers the barrier height to the

value of 333.8 cm^{-1}, which is much lower than any other values reported previously.

Because the MP2 correlation corrections are small, the higher order correlation contribution to V_b^0 must be determined. It is calculated at the coupled-cluster singles and doubles including the connected triples method [CCSD(T)] combined with the aug-cc-pCVDZ basis set and assuming that the difference ΔV_b^0[CCSD(T)] between the CCSD(T)(full) and MP2(full) energy values gives a reliable estimate of this effect. The higher order correlation effect increases the inversion barrier by ΔV_b^0[CCSD(T)] equal to 94.7 cm^{-1}.

The correction ΔV_b^0[CCSD(T)] together with V_b^0[MP2(*limit*)] of 333.8 cm^{-1} finally gives $V_b^0 = 429$ cm^{-1}. The additional vibrational correction ΔV_b(SAV) of 64 cm^{-1} provides the effective inversion barrier V_b of 493 cm^{-1}. This value falls into the range of the experimental estimates. However, we should remember that they were based on crude models of the inversion motion.

We can derive a proper flexible model from the ab initio calculations. To construct this model, all of the geometry parameters specifying the An configuration are optimized at the inversion angle varied from 0 to 40° at a step of 5°. Then, they are represented by polynomials $P_n(\rho)$ of even or odd powers, depending on the parameter symmetry, by fitting the polynomial coefficients to the optimized parameter values. In this way, the complete flexible model of the inversion motion is determined. It is sufficient to construct the kinetic energy operator of the inversion Hamiltonian by employing a purely numerical procedure of ref 58. Naturally, the inversion potential function $V_{inv}(\rho)$ is also necessary to generate the energy levels of the inversion mode. We cannot expect that $V_{inv}(\rho)$ determined for several points by very demanding ab initio calculations presented above will allow us to reproduce perfectly the observed inversion transition frequencies due to approximations inherent in the method such as additivity of the correlation corrections. Thus, it is reasonable to use slightly less-accurate ab initio potential function $V_{inv}(\rho)$ and then refine it using the experimental data. Notice that the inversion barrier V_b^0 of 501 cm^{-1} calculated at the MP2/aug-cc-pVDZ level is close to the V_b of 493 cm^{-1} estimated at a much higher level. We can use this fact to generate the approximate inversion potential function. It can be represented by the polynomial symmetric with respect to the reflection $\rho \rightarrow -\rho$, namely

$$V_{inv}(\rho) = \sum_{n=1}^{3} A_{2n}\rho^{2n} \qquad (3)$$

The values of the coefficients A_{2n}(ADZ) fitted to the MP2/aug-cc-pVDZ energy values are presented in Table 2, together with the predicted inversion frequencies. The inversion splitting of the two lowest levels is predicted very accurately. However, the quality of the results deteriorates for the frequencies involving higher inversion states.

The refined inversion potential function fitted to four observed inversion frequencies is very similar to the corresponding ab initio function$V_{inv}(\rho)$. The coefficients A_{2n} are obtained using the MP2/aug-cc-pVDZ optimized geometry to define the flexible model. To check the effect of the flexible geometry on the potential function shape, A_{2n} are also fitted using a more accurate MP2/cc-pVTZ optimized geometry. The results show that both models yield almost identical inversion potential functions. The obtained "experimental" value of the inversion barrier of 523.9 cm^{-1} is almost the same as the barrier of 524.4 cm^{-1} derived from far-infrared data by Larsen et al.[26] although their potential function reproduced higher observed frequencies with much larger errors and they assumed a rigid inversion model.

TABLE 2: Comparison of the ab Initio MP2/ADZ Inversion Potential Parameters with the Fitted Parameters Using the MP2/ADZ (fit 1) and MP2/cc-pVTZ (fit 2) Flexible Geometries of Aniline[a]

parameter	fit 1	fit 2	ab initio	observed $\nu(n \rightarrow m)$
A_2	−12 732	−12 500	−12 684	
A_4	75 049	72 150	83 457	
A_6	27 985	289 740	−38 398	
ρ_e	16.3	16.45	16.3	
V_b	523.9	523.9	500.9	
$\nu(0 \rightarrow 1)$	40.7	40.7	41.1	40.8[b]
$\nu(1 \rightarrow 2)$	381.9	381.9	368.2	381.9[b]
$\nu(0 \rightarrow 3)$	700.1	700.1	672.7	700[c]
$\nu(0 \rightarrow 4)$	1083.95	1084	1036.0	1084[d]

[a] The calculated inversion frequencies $\nu(n \rightarrow m)$ are compared to the observed ones. The A_{2n} potential coefficients are in cm^{-1}/rad^{2n}, ρ_e is in degrees, and the remaining quantities are in cm^{-1}. [b] Reference 26. [c] Reference 54. [d] Reference 14.

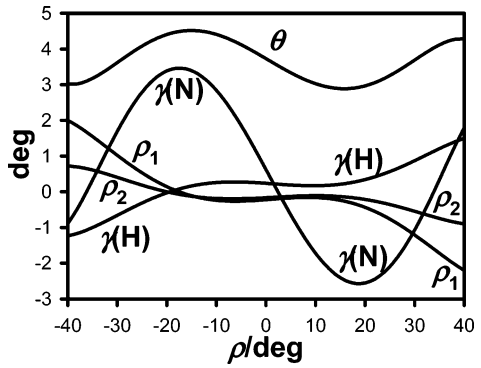

Figure 2. Flexible parameters of the AnAr complex as functions of the inversion angle ρ. The angles ρ_1 and ρ_2 specify the An ring nonplanarity, γ(N) [γ(H)] describes the tilt of the C_1−N [C_4−H] bond, and θ is the angle between the molecular z axis and the Ar position vector **r**.

IV. Inversion Motion of the Aniline−Argon Complex

The vdW interaction of Ar with the An monomer is weak; nevertheless, it is able to change qualitatively the character of the inversion motion in the AnAr complex. Theoretical analysis of this motion requires the determination of the minimum energy path along the inversion motion in the AnAr complex. This path is determined here by optimizing the AnAr geometry at the inversion angle ρ varied from −40 to + 40° at a step of 5°. The negative ρ corresponds to AnAr *anti* conformation with Ar placed over the An ring. The optimization is performed at the MP2 level with aug-cc-pVDZ basis, abbreviated further by ADZ, because it provides an accurate estimate of the vdW interaction in complexes of Ar with aromatic molecules.[59] The basis-set superposition error is automatically eliminated by the counterpoise procedure[60,61] comprised in the GAUSSIAN 03 program.

The optimized structure of the An monomer in the complex changes under vdW interaction negligibly in comparison to the isolated An structure, except for the angles defining the An nonplanarity such as the nitrogen tilt angle γ and the ring inversion angles ρ_1 and ρ_2. Their variations as functions of the amino inversion angle ρ are illustrated in Figure 2. The angle γ reaches its maximum of 3.47° at the first local potential minimum *anti* for the inversion angle ρ_e(*anti*) = −16.2° The minimum angle γ of −2.46° is achieved at the second higher

TABLE 3: Parameters of the *anti* and *syn* Potential Minima of AnAr Calculated at the MP2/ADZ ab Initio Level[a]

parameter	min(*anti*)	min(*syn*)
r_e	3.503	3.510
z_e	3.492	3.505
x_e	0.275	0.177
θ_e	4.5	2.9
ν_x	19.6	21.0
ν_y	34.6	34.6
ν_z	41.6	41.2
ZPE(vdW)	47.9	48.4
ΔE_{vib}(SAV)	3.3	5.7
D_e	453	442
D_e[CCSD(T)][b]	434	417

[a] The coordinates of the minima r_e, z_e, and x_e are in angstroms, except for the angle θ_e in degrees. The remaining quantities explained in the text are in cm^{-1}. [b] D_e is calculated at the CCSD(T)/ADZ+MB level.

potential minimum *syn* for $\rho_e(syn) = +16.2^o$. Notice that the angle $\theta(\rho)$ describing the deviation of Ar from the molecular *z* axis toward the nitrogen atom oscillates in phase with the oscillation of the angle $\gamma(\rho)$. When $\rho < 0$, the NH_2 group is strongly bent and its hydrogens push the ring carbons C_2 and C_6 up toward Ar, which is reflected in the large ρ_1 angle, cf. Figure 2. The Ar atom is repulsed by these carbon atoms at short distances and shifted toward the *z* axis. The shape of the function $\theta(\rho)$ at $\rho > 0$ can be explained similar to that at $\rho < 0$.

The calculated MP2/ADZ inversion potential function of the complex $V^0_{inv}(\rho)$ is asymmetric with the local minimum *anti* lower than the minimum *syn* by 11 cm^{-1}. This potential can be represented as a sum of the inversion potential of the unperturbed aniline and the contribution $\delta V_{inv}(\rho)$ generated by the vdW interaction of Ar with the An monomer. The function $\delta V_{inv}(\rho)$ is defined as

$$\delta V_{inv}(\rho) \equiv V^0_{inv}(\rho|\mathrm{AnAr}) - V^0_{inv}(\rho|\mathrm{An}) \qquad (4)$$

where both inversion potentials of AnAr and of An are taken as zero at $\rho = 0$. This function is approximated by the polynomial $\delta V_{inv}(\rho) = \sum_n d_n \rho^n$ with the coefficients $(d_1,d_2,d_3,d_4,d_5) = (31.4,57.7,-162.5,-96.0,152.4)$ cm^{-1}.

The properties of the inversion potential minima are compared in Table 3. In the lower minimum *anti*, the Ar atom is closer to the ring and its shift x_e from the RC point toward the N atom is larger than that in the corresponding minimum *syn*. The binding energies determined for both minima appear to be about 450 cm^{-1}. This value is larger than those determined recently for the complexes of Ar with planar benzene derivatives.[62] The difference $\Delta D_e = D_e(anti) - D_e(syn)$ in the binding energies of both minima is crucial for the inversion dynamics, so we calculated it at higher ab initio level involving the CCSD(T) method with the ADZ basis set supplemented by midbond (MB) functions 3s3p2d1f1g with exponents recommended by Koch et al.[63] The obtained binding energies are slightly lower but the difference ΔD_e of 17 cm^{-1} is larger in comparison to the MP2/ADZ value.

The vibrational frequencies of the complex, except for the inversion mode considered further, differ slightly for both minima. The vdW frequencies calculated at the MP2/ADZ method, including the counterpoise correction, were multiplied by the scale factor of 0.85 determined in ref 64 for complexes of Ar with aromatics. The scaled frequencies ν_x and ν_y (19.6 and 34.6 cm^{-1}) agree well with the corresponding frequencies (19.6 and 35.7 cm^{-1}) observed in the ArAn electronic S_0 state.[9] The frequency ν_x of the softest mode is noticeably lower for the minimum *anti* than for the minimum *syn*.

The intramolecular frequencies of the An monomer modes also differ slightly for the *anti* and *syn* minima. The An vibrational frequency shifts $\Delta\nu_i = \nu_i(\mathrm{An}) - \nu_i(\mathrm{AnAr})$ calculated at the MP2/ADZ level are positive and below 1 cm^{-1} for most of the SAV modes. This shows that the vdW interaction slightly lowers the SAV frequencies, except for the lowest out-of-plane modes. These are the C_1-N bending with $\Delta\nu_{bend}(anti) = -2.7$ and $\Delta\nu_{bend}(syn) = -2.3$ cm^{-1} and the NH_2 torsion with $\Delta\nu_{tors}(anti) = -2.4$ and $\Delta\nu_{tors}(syn) = +0.6$ cm^{-1}. A small value of $\Delta\nu_{tors}(syn)$ follows from the fact that the N atom moving during the NH_2 torsion is less sensitive to the vdW interaction in the *syn* conformer because the N−Ar distance is longer than that in the *anti* conformer.

The large sensitivity of the out-of-plane low-frequency modes to the vdW interaction has been observed in fluorescence excitation spectra in AnA complexes with A = He, Ne, Ar.[65] However, the $\Delta\nu_i$ values for the ground electronic state (S_0) could not be extracted from the spectra because the observed shifts of vibronic bands in the S_1-S_0 electronic transition contained contributions from $\Delta\nu_i(S_0)$ and $\Delta\nu_i(S_1)$.

According to eq 1, the difference in the total frequency shift ΔZPE(SAV) of the An modes contributes to the effective inversion potential $V_{inv}(\rho)$ of the AnAr complex. This potential also includes the contribution from the ZPE of the vdW modes. As a consequence, the difference $\Delta V_{inv} = V_{inv}(\rho_e) - V_{inv}(-\rho_e)$ between the inversion potential minima at ρ_e (*syn*) and $-\rho_e$ (*anti*) can be calculated as

$$\Delta V_{inv} = -[D_e(\rho_e) - D_e(-\rho_e)] - [\Delta\mathrm{ZPE}(\mathrm{SAV},\rho_e) - \Delta\mathrm{ZPE}(\mathrm{SAV},-\rho_e)] + \mathrm{ZPE}(\mathrm{vdW},\rho_e) - \mathrm{ZPE}(\mathrm{vdW},-\rho_e) \qquad (5)$$

Taking the binding energies $D_e(\pm\rho_e)$ calculated at the CCSD(T) level and the remaining data from Table 3, one obtains $\Delta V_{inv} = 15$ cm^{-1}. The function $\delta V_{inv}(\rho)$ calculated at the MP2/ADZ level gives too low of a difference of 11 cm^{-1} between two potential minima and does not contain vibrational corrections. We can approximately correct this function and convert it to the effective correction $\delta V_{eff}(\rho)$ by multiplying $\delta V_{inv}(\rho)$ by the scaling factor of 1.4 to obtain a proper value of ΔV_{inv}. Now the total effective inversion potential function of AnAr is composed of two components

$$V_{inv}(\rho|\mathrm{AnAr}) = V_{inv}(\rho|\mathrm{An}) + \delta V_{eff}(\rho) \qquad (6)$$

The An inversion potential fitted to the experimental data can be substituted to $V_{inv}(\rho|\mathrm{An})$ because it is more accurate than the corresponding ab initio potential function.

The inversion wave functions calculated from the AnAr inversion flexible model with the potential function of eq 6 give us the probability density $p_n(\rho)$, which is presented in Figure 3 for the lowest inversion states $n = 0$ and 1. It is apparent that the inversion tunneling is not completely damped by the vdW interaction. However, a small asymmetry of the inversion potential $V_{inv}(\rho|\mathrm{AnAr})$ induces a strong localization of $p_n(\rho)$. In the ground inversion state $n = 0$, the density of probability of finding AnAr at the *anti* conformation is almost three times higher than that of the *syn* conformation. The reverse situation appears in the first excited inversion state $n = 1$. Thus, the ground (excited) inversion state can be considered as a well-defined conformer *anti* (*syn*). The inversion splitting of 41.1 cm^{-1} calculated for AnAr defines the difference in the energies of these conformers.

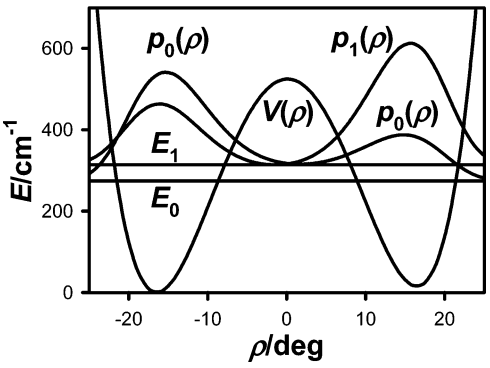

Figure 3. Inversion potential function $V_{inv}(\rho)$ of AnAr in its ground electronic state, and the probability density functions $p_n(\rho)$ for the first two inversion states $n = 0$ and 1.

V. Intermolecular Potential Energy Surface

The description of the AnAr complex can be simplified due to the fact that the inversion wave functions are localized mainly at the *anti* or *syn* local minima, as proven above. Thus, we can describe approximately the intermolecular interaction by freezing the An configurations in the *anti* and *syn* structures, which are very similar to the structure of the isolated An molecule. We checked that small distortions of the An structure by the vdW interaction in the *anti* and *syn* conformers cause a perturbation in their binding energies D_e of less than 1 cm^{-1}. As a result, the two AnAr conformers can be well described by one global intermolecular PES with two local minima generated by An in a single frozen configuration. In this picture, the inversion of the amino hydrogens is completely blocked, and the Ar atom can move above and below the An ring. This model is expected to be adequate for a description of the vibrational states of the Ar atom interacting with An monomer in the lowest inversion states.

The counterpoise-corrected interaction energy[60,61] is calculated here using the MP2/ADZ method. Recently, we proved for a series of complexes of Ar with aromatics that this method generates highly accurate interaction energies due to a mutual compensation of the MP2 correlation error and the incompleteness error of the ADZ basis set.[59,62]

The PES is sampled by varying Ar positions in a large domain. The distance r of Ar from the ring center (RC) of An is varied from 3.0 Å up to 10 Å in steps of 0.1 Å near the *anti* and *syn* minima. The polar angle θ is varied in a full range from 0° to 180° with a step size of 3° near the minima. Larger steps are taken in regions far away from the minima. The azimuthal angle ϕ is varied from 0° to 180° with steps of 30°.

The interaction energy values calculated at the chosen grid points are fitted by the analytical function $V(x,y,z)$ in the form of the many-body expansion applied successfully to other complexes.[62] The form and parameters specifying these functions are reported in the Supporting Information. The analytical PES obtained reproduces 1640 ab initio single-point energies included into the fit, from the energy range between −450 cm^{-1} and the threshold energy $E_{max} = 200$ cm^{-1} above the dissociation limit, with the standard error of 2.3 cm^{-1}.

The potential function $V(\mathbf{r})$ obtained is further improved to correct its anisotropy that has been slightly overestimated by the MP2/ADZ method, which produces overly high potential values in the ring plane.[59] Such a shortcoming can be removed by introducing a correction function $C(z)$ that transforms $V(\mathbf{r})$to a new potential function $\tilde{V}(\mathbf{r}) = V(\mathbf{r})C(z)$, which behaves properly in the ring plane. The function $C(z)$ of the form

$$C(z) = 1 + A[\exp(-\alpha z^2) - \exp(-\alpha z_e^2)] \qquad (7)$$

with $A = 0.2$ and $\alpha = 0.25$Å^{-2} as been determined in ref 59 and appeared to be approximately transferable, so it is applied to AnAr without any modifications. It is possible to use the additional correction function $\Delta V(x,y)$ to modify $V(\mathbf{r})$ near the global minimum, which is usually slightly deeper and steeper than the real one.[59] Indeed, the AnAr binding energy D_e calculated using the CCSD(T) method, which provides more accurate results than the MP2 method, appears to be slightly lower than D_e(MP2/ADZ). Instead of correcting $V(\mathbf{r})$ with the help of the $\Delta V(x,y)$ function, we simply scale the function $V(\mathbf{r})$ $C(z)$ by the factor $s_0 = D_e$[CCSD(T)]/D_e(MP2) where D_e[CCSD(T)] = 434 cm^{-1}, see Table 3. In this way, we finally obtain the potential function

$$\tilde{V}(\mathbf{r}) = s_0 V(\mathbf{r})\, C(z) \qquad (8)$$

for which the global minimum is equal to $-D_e$[CCSD(T)] for $s_0 = 0.961$.

The corrected PES is presented in Figure 4a−c. The intersection of the PES by the *xz* plane reveals two deepest potential wells, *anti* (above the An ring) and *syn* (below the An ring) and an additional shallow local minimum at $(x,y,z)_{RC} = (6.39, -0.71, 0.0)$ Å with the energy of 278 cm^{-1} above the global minimum *anti*. This minimum, located 3.67 Å from the N atom, shows properties analogous to that of the deepest minimum in the simpler NH_3Ar complex where Ar approaches nitrogen between two N−H bonds at a distance N−Ar of 3.57 Å.[66] The binding energy of 150 cm^{-1} of this minimum is very close to the corresponding value of 156 cm^{-1} for AnAr.

The PES around its global minimum *anti* shown in Figure 4b reveals a strong anisotropy in the domain of the C−N bond. The PES shape is very similar to that in the isoelectronic phenol−Ar (PhAr) complex. The same refers to secondary shallow minima placed in AnAr near its ring plane. All of these minima with the binding energies ranging from 210 to 230 cm^{-1} are localized opposite to the C−C bonds in the An ring, as shown in Figure 4c. The potential barriers separating these minima from the *anti* and *syn* minima are too low (<20 cm^{-1}) to localize the vibrational states corresponding to planar conformers. An analogous situation takes place in PhAr.

A detailed picture of the vdW interaction in AnAr compared to the interaction in the parent benzene−Ar (BAr) complex is visualized in Figure 5a and b, which presents the vdW hole[62] defined as $\Delta V_{An}(\mathbf{r}) = \tilde{V}_{An}(\mathbf{r}) - \tilde{V}_B(\mathbf{r})$ where $\tilde{V}_{An}(\mathbf{r})$ [$\tilde{V}_B(\mathbf{r})$] is the PES of the AnAr [BAr] complex. This function describes how the NH_2 group attached to the benzene ring perturbs its interaction with Ar. The vdW hole is plotted in the planes $z = z_0 = 3.5$ Å (Figure 5a) and $z = -z_0$ (Figure 5b). Both figures show large regions around the C−N bond where $\Delta V_{An}(\mathbf{r})$ takes negative values. This means that in these regions the Ar atom is more strongly attracted to the An monomer than to benzene. The vdW hole is deeper near the minimum *anti* than near the minimum *syn* at the same distance from the monomer plane. However, the interaction changes its character near the N atom because of a small tilt of the N atom above the ring plane, that is, $z(N) = +0.07$ Å. The vdW hole in AnAr is deeper than the analogous hole in PhAr. The stronger vdW

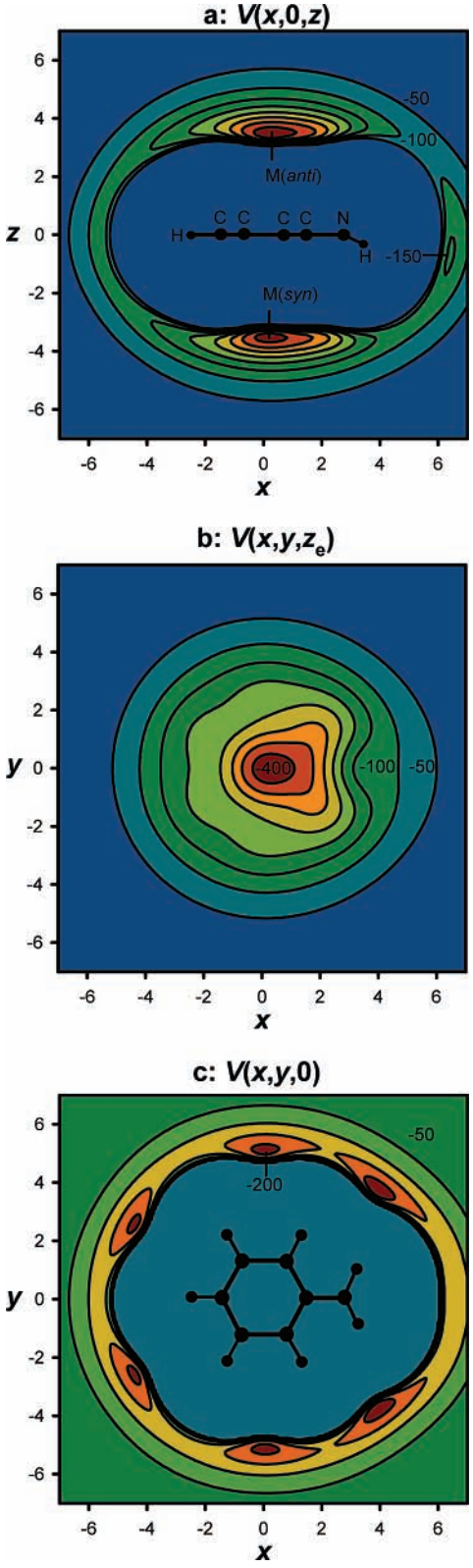

Figure 4. Contour plots of the potential energy surface $\tilde{V}(x,y,z)$ of AnAr in the *xz* plane (a), in the *xy* plane for $z = z_e = 3.481$ (b), and for $z = 0$ (c). The (x,y,z) coordinates are in angstroms, and the subsequent contours differ by 50 cm^{-1}. The sticks and balls represent the An monomer.

interaction in AnAr can be attributed to the nonzero dipole moment component μ_z perpendicular to the An ring. For Ph, $\mu_z = 0$, whereas μ_z calculated for An at the MP2/cc-pVTZ level is given by −1.12 D.

VI. Intermolecular Vibrations

The frequencies of the intermolecular vdW modes of AnAr in the ground electronic state (S_0) have been observed in the Raman spectra obtained in the molecular beam conditions,[9] where only the lowest vdW vibrational states of the most stable AnAr conformer could be populated. These states are localized in the deepest minimum of the intermolecular PES. A comparison of the vdW energy levels calculated from the PES determined with the observed frequencies can indicate which of the two conformers, *anti* or *syn*, was observed because the tunneling between these minima is unfeasible for low vdW states due to potential barriers, higher than 200 cm^{-1}, separating these minima.

The lowest vdW states of the minimum *anti*, calculated by the variational method described in ref 67, are collected in Table 4. They are assigned by approximate harmonic oscillator quantum numbers (n_x,n_y,n_z) determined with the help of the coordinate mean amplitudes $\Delta q = \langle (q - \langle q \rangle)^2 \rangle^{1/2}$ for $q = x,y,z$, vibrational density matrices,[68] and nodal patterns of the vibrational wave functions.

The ZPE of the vdW modes of 54 cm^{-1} derived from the PES, see Table 4, the ZPE correction from the An monomer modes of 3 cm^{-1}, and the binding energy of 434 cm^{-1}, taken from Table 3, give the dissociation energy $D_0(anti) = 383$ cm^{-1}. The spectroscopic estimation[12] brackets the D_0 value for the S_1 electronic state between 442 and 460 cm^{-1}. The corresponding lower and upper limit for the S_0 state can be determined from the spectral shift[11−13] of 53 cm^{-1}, which describes the increase in D_0 under electronic excitation, so $389 < D_0(S_0) < 407 cm^{-1}$. Our theoretical value is close to lower experimental D_0 limit.

However, Piest et al.[14] using their experimental data for the AnAr cation proposed significantly lower limits for $D_0(S_0)$ between 273 and 329 cm^{-1}. A comparison of the experimental value $D_0(S_0) = 364 \pm 12$ cm^{-1} for the PhAr complex[69] with the $D_0(S_0)$ upper limit of 329 cm^{-1} for the isoelectronic AnAr complex suggests that this limit is probably too low. Our theoretical method reproduced $D_0(S_0)$ for PhAr to within experimental error,[62] so the same accuracy can be expected for AnAr.

A similarity of both complexes is apparent from their vdW spectra. Table 4 contains the lowest vdW vibrational levels of the isoelectronic complexes: AnAr, PhAr, and fluorobenzene−Ar (FBAr). The calculated stretching fundamentals are identical in AnAr and PhAr, which means that the PES curvature at the minimum, along the *z* coordinate relevant to the dissociation limit, is nearly the same in these complexes.

The lowest-frequency modes in AnAr are the bending vibrations along the *x* and *y* axes. The fundamental frequencies $\nu_x(anti) = 19.6$ and $\nu_y(anti) = 35.6$ cm^{-1} of these modes calculated for the minimum *anti* are in excellent agreement with the frequencies of 19.6 and 35.7 cm^{-1} observed in the Raman spectra.[9] Note that the vdW fundamentals computed from the anharmonic PES also agree well with the corresponding scaled harmonic frequencies from Table 3. At present, the harmonic frequencies can be calculated routinely including the counterpoise correction, so the vdW fundamentals can be calculated with a reasonable accuracy at a low computational cost.

The vdW frequencies calculated earlier for the S_0 state cannot be considered as reliable. The AnAr fundamentals $(\nu_x,\nu_y,\nu_z) = (12.6, 22.0, 46.6)$ cm^{-1} calculated from an empirical PES by Parneix et al.[30] are very far from the real ones, except for the stretching fundamental.

The vdW vibrational frequencies calculated from our PES for the conformer *syn* appear to be almost the same as those

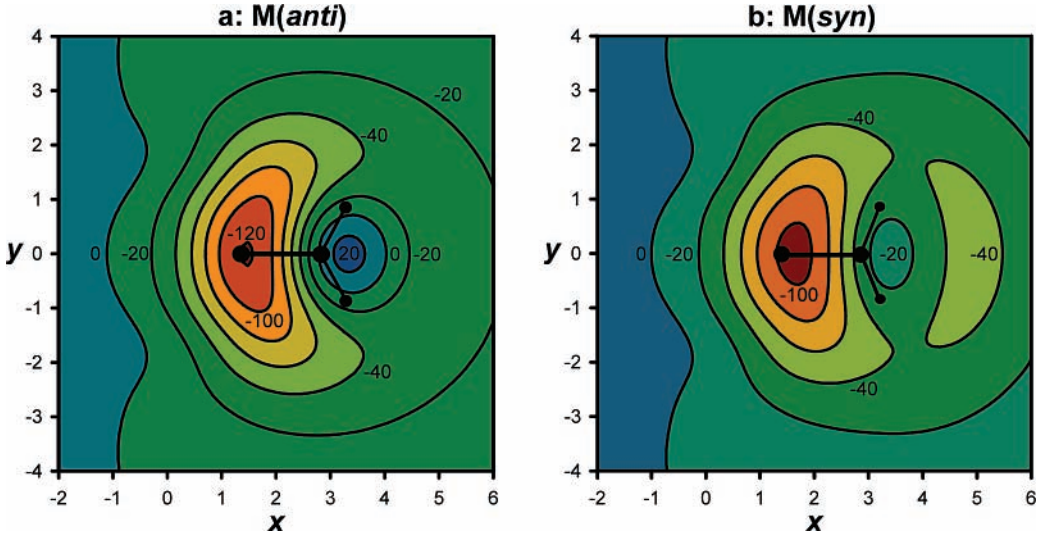

Figure 5. van der Waals potential hole in AnAr near the minimum *anti* in the plane $z = 3.5$ (a) and near the minimum *syn* in the plane $z = -3.5$ (b). The (x,y,z) coordinates are in angstroms. The potential contours are plotted with a step of 20 cm^{-1}. The sticks and balls represent the C-NH_2 group.

TABLE 4: Comparison of the AnAr, PhAr, and FBAr Vibrational vdW States in the Ground Electronic State, S_0[a]

N	$n_x n_y n_z$	$\langle\Delta x\rangle$	$\langle\Delta y\rangle$	$\langle\Delta z\rangle$	AnAr $E_{cal}(S_0)$	PhAr $E_{cal}(S_0)$[b]	FBAr $E_{cal}(S_0)$[b]
0	0 0 0	0.291	0.287	0.116	0[c]	0[d]	0[e]
1	1 0 0	0.518	0.300	0.117	19.6	21.2	21.9
2	0 1 0	0.316	0.521	0.119	35.6	34.6	33.4
3	2 0 0	0.648	0.320	0.136	36.1	36.6	37.6
4	0 0 1	0.430	0.345	0.187	44.6	44.5	45.2
5	1 1 0	0.559	0.551	0.120	52.3	53.4	53.2
6	3 0 0	0.762	0.343	0.142	52.6	51.6	53.9
7	1 0 1	0.696	0.366	0.178	64.5	61.6	64.7
8	2 1 0	0.712	0.588	0.131	66.8	66.4	67.0
9	4 0 0	0.691	0.532	0.149	68.4	68.6	69.3
10	0 2 0	0.530	0.583	0.146	69.9	67.6	65.4
11	0 1 1	0.462	0.630	0.184	75.4	73.4	73.8
12	0 0 2	0.766	0.405	0.208	79.5	81.2	80.7

[a] The calculated energies are in cm^{-1}, and coordinate amplitudes $(\Delta q)_{RC}$ of the AnAr states are in angstroms. [b] Reference 62. [c] $E_{000} = 53.8$ cm^{-1}. [d] $E_{000} = 54.2$ cm^{-1}. [e] $E_{000} = 52.9$ cm^{-1}.

for the conformer *anti*, except for the lowest bending frequency $\nu_x(syn) = 21.1$ cm^{-1}. The fact that the calculated value of $\nu_x(anti)$ matches the observed frequency perfectly indicates strongly that the *anti* conformer of the lowest energy was observed in the molecular beam.[9]

The higher vdW states show a mixed character not reflected by the approximate quantum numbers(n_x,n_y,n_z). The mode mixing is so extensive that purely excited stretching overtones do not exist in AnAr, similar to that in PhAr.[62]

A close relation between the features of vdW states and the vdW hole can be found in Table 4. The minimum value of vdW hole ΔV_{min} at the distance $z_0 = 3.5$ Å from the ring approaches the value of about $(-70, -100, -120)$ cm^{-1} in the complexes MAr = (FBAr, PhAr, AnAr), see ref 62. The increasing deformation of PES along the x coordinate lowers the bending frequency ν_x (21.9, 21.2, 19.6) cm^{-1} and simultaneously increases ν_y (33.4, 34.6, 35.6) cm^{-1} in these complexes. The relation between $\Delta V_{min}(z_0)$ and ν_x, as well as ν_y, is nearly linear.

The vdW hole affects the equilibrium structural parameters x_e and z_e. A deep vdW hole shortens the distance between the monomer ring and Ar. The relation between $z_e = (3.530, 3.510, 3.491)$ Å and $\Delta V_{min}(z_0)$ is nearly linear for MAr. The shift of Ar from the RC point $x_e = (0.113, 0.136, 0.261)$ Å, see ref 62, grows faster than linearly with the increase of $\Delta V_{min}(z_0)$.

TABLE 5: Assignments of the Vibrational vdW Frequencies (cm^{-1}) of AnAr in the S_1 Electronic State

$n_x n_y n_z$	expl[a]	calc this work	expl[b]	calc → expt[c]
1 0 0	22.1	22.6	22	18.1 → 22.1
0 1 0	37.7	37.6		
2 0 0	39.6	40.3	41	33.8 → 37.7
0 0 1	47.8	48.2	49	42.3 → 39.6
0 2 0		73.5	39	53.6 → 47.8

[a] Reference 13. [b] Assignment of the observed frequencies by Bieske et al.[6] [c] Assignment of the calculated frequencies[30] to the observed ones[13] according to the quantum numbers from column 1.

The excited states involving the vdW stretching mode have been observed in the S_1-S_0 vibronic spectra; however, there is still disagreement between alternative assignments of these spectra.[6,7] The knowledge of the accurate PES for the S_0 electronic state can help us solve the assignment problem because the PES for the S_1 electronic state usually does not differ much from PES(S_0). The approximate PES(S_1) can be obtained by a simple modification of PES(S_0). Here, we take into account only the two most important properties that change under the electronic excitation, namely, the equilibrium geometry of the An monomer, which becomes planar in the S_1 state, and the binding energy, which increases under electronic excitation. The observed spectral shift of 53 cm^{-1} is approximately equal to the increase in the potential well depth in the S_1 state. The PES(S_1) with the binding energy $D_e(S_1)$ larger by 53 cm^{-1} than $D_e(S_0)$ is obtained by increasing the scaling factor s_0 in eq 8 to the new value $s_1 = 1.08$.

The modified potential function $\tilde{V}_{S_1}(\mathbf{r}) = s_1 V(\mathbf{r})\ C(z)$ is obtained using the An planar structure. The vdW vibrational frequencies determined from $\tilde{V}_{S_1}(\mathbf{r})$ are ascribed to the vdW frequencies measured in the S_1 state by Douin et al.[13] in Table 5. The theoretical frequencies are systematically higher than the observed ones by about 0.5 cm^{-1}, except for ν_y that is even better estimated. Such a high accuracy achieved by introduction of only one well-defined parameter s_1 is a strong argument in favor of our assignment. The assignment of Bieske et al.[6] was correct, except for the frequency of 39 cm^{-1} ascribed to the overtone $2\nu_y$ instead of to ν_y. According to the Franck−Condon rule, the fundamental ν_y should not be observed because of its symmetry lower than a_1. However, this rule does not apply strictly to floppy molecular complexes.

TABLE 6: Comparison of the MPA Coordinates (in angstroms) of Ar in AnAr Determined from the Empirical r_0, r_s, and r_{eff} Models[a] with the Coordinates Calculated from the ab Initio Potential Function $\tilde{V}(\mathbf{r})$

parameter	$\tilde{V}(\mathbf{r})$	r_{eff}	r_0	$\lvert r_s\rvert$
x_e	−0.192	−0.163		
z_e	3.487	3.535		
r_e	3.493	3.539		
$\langle x\rangle$	−0.111		−0.260	
$\langle z\rangle$	3.533		3.524	
$\langle r\rangle$	3.560		3.544	
$\langle x^2\rangle^{1/2}$	0.312			0.235
$\langle y^2\rangle^{1/2}$	0.287			0.392
$\langle z^2\rangle^{1/2}$	3.535			3.516

[a] Reference 5.

The assignment of Hermine et al.,[7] supported further by Parneix et al.[30] and Douin et al.,[13] who attempted to revise Bieske's assignment, appears to be incorrect. These authors based their interpretation on the theoretical frequencies calculated from a crude empirical PES constructed as a sum of two-body interactions, supplemented by an induction term. However, a realistic PES should include higher many-body terms, as demonstrated in this paper.

The knowledge of PES allows us to determine the vibrationally averaged structures of the complex and compare them to the corresponding structures determined from the experiment. The equilibrium AnAr structure r_e of the global minimum (*anti*) is described in Table 6. The equilibrium Ar coordinates $q_e = x_e, y_e, z_e$ together with the expectation values $\langle q\rangle_0$ and $\langle q^2\rangle_0^{1/2}$ of the ground vibrational state calculated for the *anti* conformer are given with respect to the monomer center of mass. The "experimental" coordinates are usually reported in the monomer principal axis (MPA) system. For this reason, the ab initio coordinates calculated in the molecular axis system with the x axis attached to the C_4-C_1 axis, as shown in Figure 1, are transformed to the MPA coordinates.

The molecular structure is not directly observable, and the physical meaning of the "experimental structure" depends on the model used in its derivation from the experimental data. The most accurate rotational constants obtained from the microwave spectra of AnAr and its ^{15}N-isotopomer have been used to determine the r_0, r_s, and r_{eff} structures of this complex.[4,5] The r_0 structure can be interpreted approximately as a vibrationally averaged structure defined by the coordinate expectation values $\langle q\rangle_0$ for the ground vibrational state. The coordinates $|q_s|$ defining the r_s substitution structure of AnAr have been determined from Kraitchman's equations.[70] This kind of coordinate can be interpreted[2] as zero-point root mean squares $\langle q^2\rangle_0^{1/2}$. The coordinates $|q_{eff}|$ of the effective structure r_{eff} have been determined using the model of Klots,[71] modified by Spycher.[72] This model incorporates partly the flexibility of the complex; thus, the r_{eff} structure is expected to be close to the equilibrium structure, r_e, defined by the global potential energy minimum.

The coordinate x_{eff} compares reasonably with the calculated equilibrium coordinate x_e; however, the coordinate z_{eff} is much too large. It is even larger than z_0 and z_s that contain the vibrational contribution from the amplitude of the stretching mode. However, z_0 and z_s agree well with the theoretical values of $\langle z\rangle_0$ and $\langle z^2\rangle_0^{1/2}$.

The empirical parameters x_0 and x_s corresponding to $\langle x\rangle_0$ and $\langle x^2\rangle_0^{1/2}$ have large errors of the order of 0.1 Å. This estimation follows from the fact that x_s, which includes the vibrational contribution from the softest bending x mode, should be larger than y_s associated to the y mode of the higher frequency. However, x_s determined for AnAr is much smaller than y_s. This clearly indicates that these empirical parameters do not reflect the real structure of the complex correctly. The corresponding ab initio parameters $\langle x^2\rangle_0^{1/2}$ and $\langle y^2\rangle_0^{1/2}$ are consistent and reliable because they are calculated from the PES that describes the vibrational modes very accurately.

Notice that inconsistencies in the empirical structural parameters shown above follow from different simplifying assumptions inherent in the empirical models. As a consequence, it was difficult to establish the real structure of the complex unambiguously.

VII. Summary and Conclusions

The present ab initio study of the structure and dynamics of the An monomer and its complex with Ar have provided detailed information on the inversion motion consistent with the experimental data available. The An inversion barrier height, V_b, has been estimated by determining the contributions from the electronic energy and vibrational corrections. Accurate determination of the inversion potential in the AnAr complex perturbed by the weak vdW interaction required additional contributions from the ZPE of the vdW modes and from the SAV frequency shifts generated by the complexation. The resulting asymmetrical inversion potential shows two local minima corresponding to the *anti* and *syn* AnAr conformers. Although the difference in their energies approaches only 15 cm^{-1}, it is sufficient to localize strongly the inversion wave functions of two lowest states.

The three-dimensional PES of the complex has been constructed from a large set of single-point interaction energies calculated using the MP2/ADZ method. This PES reveals several local minima surrounding the An molecule. A simple rule explaining qualitatively the locations of all of the minima can be formulated as follows. The Ar atom approaches the heavy atoms A of the monomer molecule at a typical Ar−A distance of about 3.5 Å and prefers to occupy the space regions far from the hydrogens to avoid their repulsion at too close Ar−H distances. Thus, Ar intrudes into a company of the heavy atoms in between the A−H bonds. The minima located near the monomer plane are very shallow and are separated by low potential barriers, so stable conformers corresponding to such minima cannot be formed. Naturally, there is a plenty of space free from hydrogens above and below the monomer ring and there the local minima are the deepest. This rule applies to all neutral complexes of Ar with aromatics studied so far.[62]

The shape of the PES of AnAr is similar to that of the parent benzene−Ar cluster. However, it is appreciably deformed by the NH_2 group attached to the phenyl ring. The vdW hole describing this effect is pronounced in the region around the C−N bond, and this hole is responsible for important dynamical features of the excited vdW vibrational states. The interesting relations between the vdW hole and the structural and dynamical properties are found in the series of isoelectronic complexes MAr = (BFAr, PhAr, AnAr) with increasing vdW hole depth $\Delta V_{min}(z_0)$ at the same fixed coordinate z_0.

The vdW bending fundamentals calculated for the minimum *anti* are in excellent agreement with the vibrational frequencies observed in the ground electronic state,[9] and this proves the high accuracy of the PES determined. The vdW vibrational levels predicted for the excited electronic state (S_1) have permitted the explanation of the structure of the observed vibronic bands, and their assignments as proposed earlier have now been corrected.

The ab initio structural parameters have been calculated from the PES allowing a careful analysis of the experimental structures derived earlier using simplified models.

All controversies concerning the structure and dynamics of the AnAr complex have been resolved by a careful analysis of the subtle effects not considered earlier.

Acknowledgment. I thank Dr. Alan Salter and Prof. Andrzej Wierzbicki for critically reading the manuscript. A part of the calculations was performed at the Poznan Supercomputing and Networking Center.

Supporting Information Available: The An geometry in the S_0 and S_1 electronic states, the An and AnAr vibrational fundamental frequencies, and the analytical PES of AnAr. This material is available free of charge via the Internet at http://pubs.acs.org.

References and Notes

(1) Yamanouchi, K.; Isogal, S.; Tsuchiya, S.; Kuchitsu, K. *Chem. Phys.* **1987**, *116*, 123.
(2) Becucci, M.; Pietraperzia, G.; Lakin, N. M.; Castellucci, E.; Bréchignac, Ph. *Chem. Phys. Lett.* **1996**, *260*, 87.
(3) Sinclair, W.; Pratt, D. *J. Chem. Phys.* **1996**, *105*, 7942.
(4) Consalvo, D.; Storm, V.; Dreizler, H. *Chem. Phys.* **1998**, *228*, 301.
(5) Storm, V.; Dreizler, H.; Consalvo, D. *Chem. Phys.* **1998**, *237*, 395.
(6) Bieske, E. J.; Rainbird, M. W., Atkinson, I. M.; Knight, A. E. W. *J. Chem. Phys.* **1989**, *91*, 752.
(7) Hermine, P.; Parneix, P.; Coutant, B.; Amar, F. G.; Bréchignac, Ph. *Z. Phys. D* **1992**, *22*, 529.
(8) Takahashi, M.; Ozeki, H.; Kimura, K. *J. Chem. Phys.* **1992**, *96*, 6399.
(9) Maxton, P. M.; Schaeffer, M. W.; Ohline, S. M.; Kim, W.; Venturo, V. A.; Felker, P. M. *J. Chem. Phys.* **1994**, *101*, 8391.
(10) Jäckel, J. G.; Jones, H. *Chem. Phys.* **1999**, *247*, 321.
(11) Amirav, A.; Even, U.; Jortner, J.; Dick. B. *Mol. Phys.* **1983**, *49*, 899.
(12) Nimlos, M. R.; Young, M. A.; Bernstein, E. R.; Kelley, D. F. *J. Chem. Phys.* **1989**, *91*, 5268.
(13) Douin, S.; Parneix, P.; Amar, F. G.; Bréchignac, Ph. *J. Phys. Chem. A* **1997**, *101*, 122.
(14) Piest, H.; Von, Helden, G.; Meijer, G. *J. Chem. Phys.* **1999**, *110*, 2010.
(15) Zhang, X.; Smith, J. M.; Knee, J. L. *J. Chem. Phys.* **1992**, *97*, 2843.
(16) Smith, J. M.; Zhang, X.; Knee, J. L. *J. Chem. Phys.* **1993**, *99*, 2550.
(17) Bieske, E. J.; Rainbird, M. W.; Knight, A. E. W. *J. Chem. Phys.* **1991**, *94*, 7019.
(18) Bieske, E. J.; Uichanco, A. S.; Rainbird, M. W.; Knight, A. E. W. *J. Chem. Phys.* **1991**, *94*, 7029.
(19) Pino, T.; Parneix, P.; Douin, S.; Bréchignac, Ph. *J. Chem. Phys.* **2004**, *108*, 7364, and references therein.
(20) Parneix, P.; Bréchignac, Ph.; Amar, F. G. *J. Chem. Phys.* **1996**, *104*, 983.
(21) Parneix, P.; Bréchignac, Ph. *J. Chem. Phys.* **1998**, *108*, 1932.
(22) Parneix, P.; Amar, F. G.; Bréchignac, Ph. *Chem. Phys.* **1998**, *239*, 121.
(23) Brand, J. C. D.; Williams, D. R.; Cook, T. J. *J. Mol. Spectrosc.* **1966**, *20*, 359.
(24) Christoffersen, J.; Hollas, J. M.; Kirby, G. H. *Mol. Phys.* **1969**, *16*, 441.
(25) Quack, M.; Stockburger, M. *J. Mol. Spectrosc.* **1972**, *43*, 87.
(26) Larsen, N. W.; Hansen, E. L.; Nicolaisen, F. M. *Chem. Phys. Lett.* **1976**, *43*, 584.
(27) Kydd R. A.; Krüger, P. J. *Chem. Phys. Lett.* **1977**, *49*, 539.
(28) Lopez-Tocón, I.; Otero, J. C.; Becucci, M.; Pietraperzia, G.; Castellucci, E. *Chem. Phys.* **1999**, *249*, 113.
(29) Lopez-Tocón, I.; Otero, J. C.; Becucci, M.; Pietraperzia, G.; Castellucci, E.; Bréchignac, Ph. *Chem. Phys.* **2001**, *269*, 29.
(30) Parneix, P.; Halbberstadt, N.; Bréchignac, Ph.; Amar, F. G.; van der Avoird, A.; van Bladel, J. W. I. *J. Chem. Phys.* **1993**, *98*, 2709.
(31) Pyka, J.; Kręglewski, M. *J. Mol. Spectrosc.* **1985**, *109*, 207.
(32) Bludsky, O.; Šponer, J.; Leszczyński J.; Špirko, V.; Hobza, P. *J. Chem. Phys.* **1996**, *105*, 11042, and references therein.
(33) Handy, N. C.; Carter, S.; Colwell, S. M. *Mol. Phys.* **1999**, *96*, 477.
(34) Makarewicz, J.; Skalozub, A. *Spectrochim. Acta, Part A* **2002**, *158*, 601.
(35) Lister, D. G.; Tyler, J. K.; Hog, J. H.; Larson, N. W. *J. Mol. Struct.* **1974**, *23*, 253.
(36) Dunning, T. H. Jr. *J. Chem. Phys.* **1989**, *90*, 1007.
(37) Frisch, M. J.; Trucks, G. W.; Schlegel, H. B.; Scuseria, G. E.; Robb, M. A.; Cheeseman, J. R.; Montgomery, J. A., Jr.; Vreven, T.; Kudin, K. N.; Burant, J. C.; Millam, J. M.; Iyengar, S. S.; Tomasi, J.; Barone, V.; Mennucci, B.; Cossi, M.; Scalmani, G.; Rega, N.; Petersson, G. A.; Nakatsuji, H.; Hada, M.; Ehara, M.; Toyota, K.; Fukuda, R.; Hasegawa, J.; Ishida, M.; Nakajima, T.; Honda, Y.; Kitao, O.; Nakai, H.; Klene, M.; Li, X.; Knox, J. E.; Hratchian, H. P.; Cross, J. B.; Bakken, V.; Adamo, C.; Jaramillo, J.; Gomperts, R.; Stratmann, R. E.; Yazyev, O.; Austin, A. J.; Cammi, R.; Pomelli, C.; Ochterski, J. W.; Ayala, P. Y.; Morokuma, K.; Voth, G. A.; Salvador, P.; Dannenberg, J. J.; Zakrzewski, V. G.; Dapprich, S.; Daniels, A. D.; Strain, M. C.; Farkas, O.; Malick, D. K.; Rabuck, A. D.; Raghavachari, K.; Foresman, J. B.; Ortiz, J. V.; Cui, Q.; Baboul, A. G.; Clifford, S.; Cioslowski, J.; Stefanov, B. B.; Liu, G.; Liashenko, A.; Piskorz, P.; Komaromi, I.; Martin, R. L.; Fox, D. J.; Keith, T.; Al-Laham, M. A.; Peng, C. Y.; Nanayakkara, A.; Challacombe, M.; Gill, P. M. W.; Johnson, B.; Chen, W.; Wong, M. W.; Gonzalez, C.; Pople, J. A. *Gaussian 03*, revision B.04; Gaussian, Inc.: Wallingford, CT, 2004.
(38) Hollas, J. M.; Howson, M. R.; Ridley, T.; Halonen, L. *Chem. Phys. Lett.* **1983**, *98*, 611.
(39) Honda, Y.; Hada, M.; Ehara, M.; Nakatsuji, H. *J. Chem. Phys.* **2002**, *117*, 2045.
(40) Hegarty, D.; Robb, M. A. *Mol. Phys.* **1979**, *38*, 1795.
(41) Roos, B. O.; Taylor, P. R.; Siegbahn, P. E. M. *Chem. Phys.* **1980**, *48*, 157.
(42) Schlegel, H. B.; Robb, M. A. *Chem. Phys. Lett.* **1982**, *93*, 43.
(43) Korter, T. M.; Borst, D. R.; Butler, C. J.; Pratt, D. W. *J. Am. Chem. Soc.* **2001**, *123*, 96.
(44) Woon, D. E.; Dunning, T. H., Jr. *J. Chem. Phys.* **1993**, *98*, 1358.
(45) Wang, S.; Schaefer, H. F., III *J. Chem. Phys.* **2006**, *124*, 044303.
(46) Jensen, P.; Bunker, P. R. *J. Mol. Spectrosc*. **1986**, *118*, 18, and references therein.
(47) Boese, A. D.; Martin, J. M. L. *J. Phys. Chem. A* **2004**, *108*, 3085.
(48) Barone, V. *J. Phys. Chem. A* **2004**, *108*, 4146.
(49) Boese, A. D.; Klopper, W.; Martin, J. M. L. *Int. J. Quantum Chem.* **2005**, *104*, 830.
(50) Hamprecht, F. A.; Cohen, A. J.; Tozer, D. J.; Handy, N. C. *J. Chem. Phys.* **1998**, *109*, 6264.
(51) Baker, J. A.; Jarzecki, A.; Pulay, P. *J. Phys. Chem. A* **1998**, *102*, 1412.
(52) Zierkiewicz, W.; Michalska, D.; Zeegers-Huyskens, Th. *J. Phys. Chem. A* **2000**, *104*, 11685.
(53) Wojciechowski, P. M.; Zierkiewicz, W.; Michalska, D.; Hobza, P. *J. Chem. Phys.* **2003**, *118*, 10900.
(54) Gée, Ch.; Douin, S.; Crépin, C.; Bréchignac, Ph. *Chem. Phys. Lett.* **2001**, *338*, 130.
(55) Nakanaga, T.; Ito, F.; Miyawaki, J.; Sugawara, K.; Takeo, H. *Chem. Phys. Lett*. **1996**, *261*, 414.
(56) Evans, J. C. *Spectrochim. Acta* **1960**, *16*, 428.
(57) Helgaker, T.; Klopper, W.; Koch, H.; Noga, J. *J. Chem. Phys.* **1997**, *106*, 9639.
(58) Makarewicz, J. In *Computational Molecular Spectroscopy*; Jensen, P.; Bunker, P. R., Ed.; Wiley: Chichester, 2000.
(59) Makarewicz, J. *J. Chem. Phys.* **2004**, *121*, 1390.
(60) Boys, S. F.; Bernardi, F. *Mol. Phys.* **1970**, *19*, 553.
(61) Simon, S.; Duran, M.; Dannenberg, J. J. *J. Chem. Phys.* **1996**, *105*, 11024.
(62) Makarewicz, J. *J. Chem. Phys*. **2006**, *124*, 084310, and references therein.
(63) Koch, H.; Christiansen, O.; Fernández, B. *J. Chem. Phys.* **1998**, *108*, 2784.
(64) Makarewicz, J. *J. Chem. Phys.* **2005**, *123*, 154302.
(65) Coutant, B.; Bréchignac, Ph. *J. Chem. Phys.* **1994**, *100*, 7087.
(66) Schmuttenmaer, C. A.; Cohen, R. C.; Sykally, R. J. *J. Chem. Phys.* **1994**, *101*, 146.
(67) Makarewicz, J.; Bauder, A. *Mol. Phys*. **1995**, *84*, 853.
(68) Makarewicz, J. *Mol. Phys.* **1989**, *66*, 113.
(69) Dessent, C. E. H.; Haines, S. R.; Müller-Dethlefs, K. *Chem. Phys. Lett.* **2000**, *315*, 103.
(70) Kraitchman, J. *Am. J. Phys* **1953**, *21*, 17.
(71) Klots, T. D.; Emilsson, T.; Ruoff, R. S.; Gutowsky, H. S. *J. Phys. Chem.* **1989**, *93*, 1255.
(72) Spycher, R. M. Ph.D. Thesis, Zürich, 1994.